Journal of Power Sources 250 (2014) 372–378

Contents lists available at ScienceDirect

Journal of Power Sources

journal homepage: www.elsevier.com/locate/jpowsour

Graphene oxide wrapped croconic acid disodium salt for sodium ion battery electrodes

Chao Luo [a], Yujie Zhu [a], Yunhua Xu [a], Yihang Liu [a], Tao Gao [a], Jing Wang [b], Chunsheng Wang [a,*]

[a] Department of Chemical and Biomolecular Engineering, University of Maryland, College Park, MD 20742, USA
[b] School of Materials Science & Engineering, Jiamusi University, 154007, PR China

HIGHLIGHTS

- Croconic acid disodium salt (CADS) is firstly used as an anode in Na-ion battery.
- The capacity decay of CADS electrode is due to particle pulverization.
- Reducing particle size is an effective approach to enhance battery performance.
- Graphene oxide wrapped CADS exhibits the best electrochemical performance.

ARTICLE INFO

Article history:
Received 6 August 2013
Received in revised form
26 October 2013
Accepted 28 October 2013
Available online 14 November 2013

Keywords:
Sodium ion batteries
Croconic acid disodium salt
Graphene oxide
Ultrasonic spray pyrolysis
Particle pulverization

ABSTRACT

Croconic acid disodium salt (CADS), a renewable or recyclable organic compound, is investigated as an anode material in sodium ion battery for the first time. The pristine micro-sized CADS delivers a high capacity of 246.7 mAh g^{-1}, but it suffers from fast capacity decay during charge/discharge cycles. The detailed investigation reveals that the severe capacity loss is mainly attributed to the pulverization of CADS particles induced by the large volume change during sodiation/desodiation rather than the generally believed dissolution of CADS in the organic electrolyte. Minimizing the particle size can effectively suppress the pulverization, thus improving the cycling stability. Wrapping CADS with graphene oxide by ultrasonic spray pyrolysis can enhance the integration and conductivity of CADS electrodes, thus providing a high capacity of 293 mAh g^{-1}.

1. Introduction

Sodium ion batteries are the most promising alternatives to lithium ion batteries due to the low cost and abundance of sodium element in the earth [1]. The chemical similarity of sodium ion toward lithium ion enables some electrode materials used in Li ion batteries to be applied for Na ion batteries [2]. Inorganic materials synthesized through energy-demanding ceramic processes [3] are the most common Li ion electrode materials. However, to satisfy the emerging large-scale applications of energy storage, next generation battery electrodes should be made from renewable or recyclable resources via low energy consumption processes. One possible approach is to use electrode materials fabricated from biomass or recyclable organic materials via solution phase routes [4].

Several organic materials have been investigated as electrodes for Li ion batteries [5], but very few organic materials were explored for Na-ion batteries. The organic electrodes face two major challenges in organic electrolyte batteries: (1) low power density due to poor electronic conductivity of organic compounds, (2) fast capacity decay during charge/discharge cycles which is generally attributed to dissolution of organic compounds into organic electrolytes [3]. One way to mitigate the dissolution of organic materials in organic electrolytes is use of organic salts [3]. Among the salts, carbonyl group based organic compounds such as lithium salt of tetrahydroxy–benzoquinone [6], lithium ethoxycarbonyl-based compound [7], dilithium trans–trans-muconate and dilithium terephthalate [8] have been investigated as electrodes for Li ion batteries. These organic salts normally contain more than two carbonyl groups which are connected by conjugated carbon matrix. These carbonyl groups are redox centers which enable the electrochemical reaction to take place in the electrodes. During the discharge process, each carbonyl group can obtain an

* Corresponding author.
E-mail address: cswang@umd.edu (C. Wang).

0378-7753/$ – see front matter © 2013 Elsevier B.V. All rights reserved.
http://dx.doi.org/10.1016/j.jpowsour.2013.10.131

electron and a lithium ion that induces electron transfer in the conjugated carbon matrix. The reaction between carbonyl group and lithium ion enables the ion transfer and electron transfer in Li ion batteries. Although the solubility of organic salts in the electrolyte has been reduced, these organic salts still suffer from fast and continuous capacity decline during charge/discharge cycles [6–8]. The mechanism behind the fast capacity decline is still not fully understood.

Most reported organic salts experience phase transformation during lithiation/delithiation as evidenced by a flat voltage plateau in charge/discharge profile and structure change in X-ray diffraction (XRD) patterns [8]. The phase transformation is normally accompanied with volume change. The large volume expansion in the first lithiation can even change the crystal structure of organic salts into amorphous structure and retain amorphous structure in the following charge/discharge cycles [8], which is also observed in Si anodes [9]. The structure change of Si from crystal to amorphous structure is attributed to the large volume change (300%) of Si during lithiation [9]. The severe volume change of Si pulverizes the Si particle, resulting in rapid capacity decline during charge/discharge cycles [10]. Therefore, the volume change of organic salts during lithiation/delithiation may be also responsible for the capacity decay.

In principle, the carbonyl group based organic electrode compounds used in lithium ion batteries can potentially be applied to sodium ion batteries [11]. However, due to larger ion size of Na^+ than Li^+, only few organic salts are suitable for Na ion batteries. In addition, the larger ion size of Na^+ causes much more severe volume change of organic salts, resulting in fast capacity decay of organic compounds in Na ion batteries [11c]. Therefore, only few organic compounds were explored for Na-ion batteries. Due to the large volume change, these organic compounds showed quick capacity decline during Na insertion/extraction [11c]. However, how the volume change of organic salts affects the cycling stability has not been investigated yet.

In this paper, croconic acid disodium salt (CADS) is used as a model electrode to investigate the capacity decline mechanism of organic salt electrodes in Na ion batteries. To our best knowledge, CADS has never been studied as a battery electrode material in Li-ion and Na-ion batteries. In addition, this is also the first effort to study the effects of phase change on capacity decay of organic salt electrodes in Na ion batteries. As shown in Fig. 1, three CADS samples, micro-sized pristine CADS, submicrometer-size CADS (sCADS), and graphene oxide wrapped CADS (GO-CADS), are employed to investigate their electrochemical behaviors toward Na. sCADS and GO-CADS are fabricated by ultrasonic spray pyrolysis.

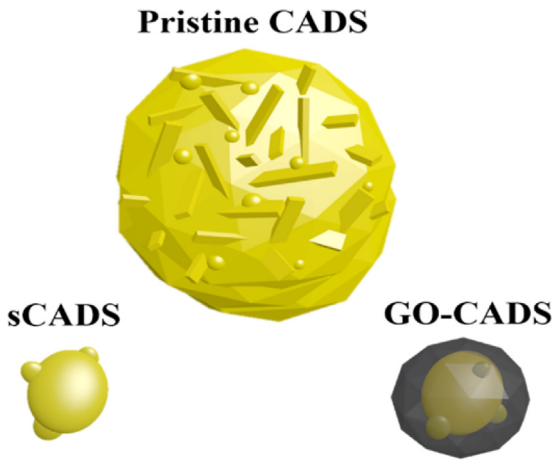

Fig. 1. Schematic illustration for pristine CADS, sCADS and GO-CADS.

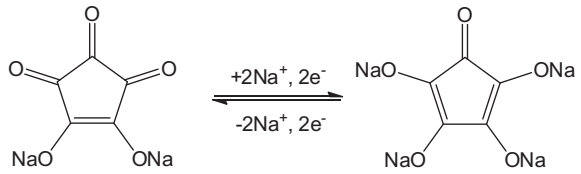

Scheme 1. The sodiation/de-sodiation mechanism for croconic acid based molecule.

Our results show that the particle pulverization is a main reason for capacity decline. Minimizing particle size and wrapping CADS with graphene oxide can effectively stabilize the electrodes during Na ion insertion/extraction, thus improving the cycling stability.

2. Experimental

All chemicals were purchased from Sigma Aldrich and used as received. The CADS with small particle size of 0.5–1.0 μm (denote

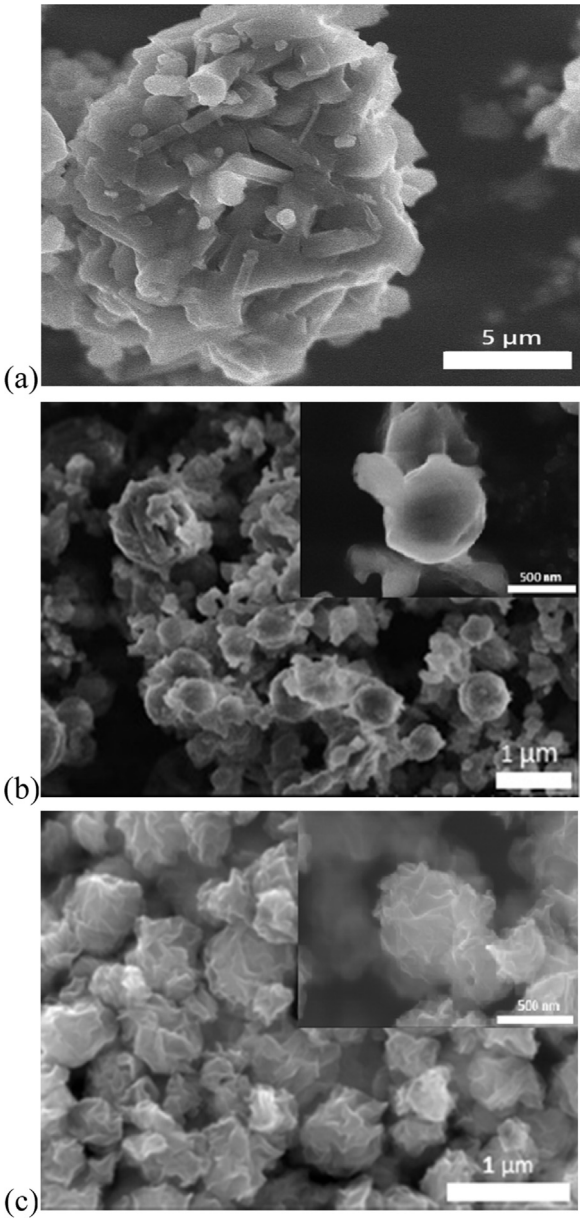

Fig. 2. The SEM images of pristine CADS (a), sCADS (b), and GO-CADS (c).

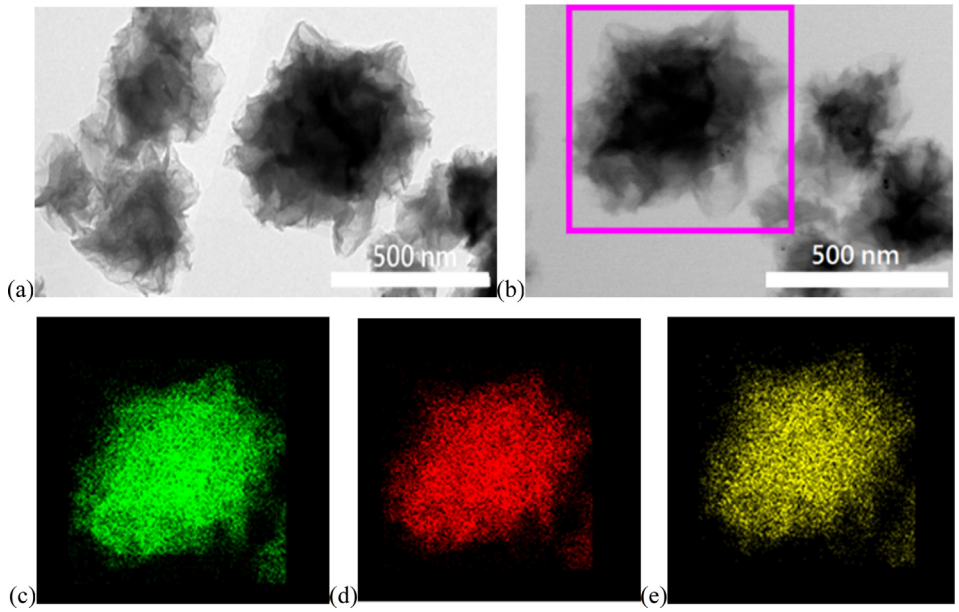

Fig. 3. TEM images of GO-CADS (a, b) and EDS elemental mapping images of the GO-CADS particle, marked by purple square in (b), for carbon (c), oxygen (d) and sodium (e). (For interpretation of the references to color in this figure legend, the reader is referred to the web version of this article.)

as sCADS) was prepared by an ultrasonic spray pyrolysis method [12]. The ultrasonic spray pyrolysis apparatus consisted of ultrasonic droplet generator, tube furnaces, and filtration system for particle collection. The ultrasonic generator operated 1.7 MHz frequency atomized the precursor solution to droplets with average diameter of approximately 1 microns. Two tube furnaces were connected in series with a total length of 81 cm. Particle collection was set at the end of the system, allowing gas to pass through and collecting particles. 200 mg CADS with average particle size of 5 μm were dissolved into 10 mL water. Aerosol droplets containing the dissolved precursors were generated using compressed nitrogen gas at a pressure of 35 psi in a collision type atomizer. The geometric mean diameter of the droplets was measured to be ~1 μm by a laser aerosol spectrometer. The produced aerosol droplets passed through a silica-gel diffusion dryer and a tube furnace preheated to 200 °C to remove most of the solvent. The products were collected on a 0.4 μm (pore size) DTTP Millipore filter and dried in a vacuum oven at 100 °C overnight.

Graphene oxide was synthesized following the modified hummer's method [13]. The graphene oxide wrapped CADS was also synthesized using ultrasonic spray pyrolysis. 100 mg CADS were dissolved in 100 mL graphene oxide aqueous solution to prepare the precursor. Nitrogen gas (2.5 L min^{-1} flow rate) was used to carry the solution droplets to the furnace series which was operated at 200 °C. In the furnace, water was evaporated, and then graphene wrapped CADS particles were generated in a residential time around 1.5 s.

Scanning electron microscopy (SEM) image was taken by Hitachi SU-70 analytical ultra-high resolution SEM (Japan); Transmission electron microscopy (TEM) images were taken by JEOL (Japan) 2100F field emission TEM; X-ray diffraction (XRD) pattern was recorded by Bruker Smart1000 (Bruker AXS Inc., USA) using CuKα radiation; Fourier transform infrared spectroscopy (FTIR) was recorded by NEXUS 670 FT-IR Instrument; UV/vis spectra were recorded on an UV-1700 spectrophotometer; Thermogravimetric analysis (TGA) was carried out using a thermogravimetric analyzer (TA Instruments, USA) with a heating rate of 10 °C min^{-1} in argon.

The CADS and sCADS were mixed with carbon black and Polyvinylidene fluoride (PVDF) binder to form slurry at the weight ratio of 45:45:10, separately. The GO-CADS was mixed with carbon black and Polyvinylidene fluoride (PVDF) binder to form slurry at the weight ratio of 70:20:10. The electrode was prepared by casting the slurry onto copper foil using a doctor blade and dried in a vacuum oven at 100 °C overnight. The electrode was cut into circular pieces with diameter of 1.2 cm for coin cell testing. Na ion batteries were assembled with sodium metal as the counter electrode, 1 M $NaClO_4$ in a mixture of ethylene carbonate/dimethyl carbonate (EC/DMC, 1:1 by volume) as the electrolyte, and Celgard® 3501 (Celgard, LLC Corp., USA) as the separator. Electrochemical performance was tested using Arbin battery test station (BT2000, Arbin Instruments, USA). 0.7 V and 2.0 V (vs. Na/Na^+) were used as low and high cutoff voltages for the galvanostatic tests. After the cell reached the cutoff voltage, it was rested for 10 min for subsequent charge or discharge. Both the charge–discharge current density and specific capacity were calculated on the basis of the mass of CADS in the electrode. Cyclic voltammogram at a scan rate of 0.1 mV s^{-1} between 0.7 and 2 V (versus Na/Na^+) was recorded using Solatron 1260/1287 Electrochemical Interface (Solatron Metrology, UK).

3. Results and discussion

3.1. Morphology and structure

Croconic acid disodium salt has a five-member ring structure with three carbonyl groups and a carbon–carbon double bond (Scheme 1). Its chemical structure is very similar to dilithium rhodizonate which has been reported as an organic electrode for Li ion batteries [4]. The carbonyl groups in this compound are redox centers which can react with Na ions and gain electrons through the reaction as shown in Scheme 1. During the sodiation, each carbonyl group, connected by the carbon–carbon double bond, gains a sodium ion and an electron. At the meanwhile, the carbon–carbon double bond is broken, and two new carbon–carbon double bonds are generated. During the desodiation, CADS molecule is recovered. The reversible reaction between CADS molecule and

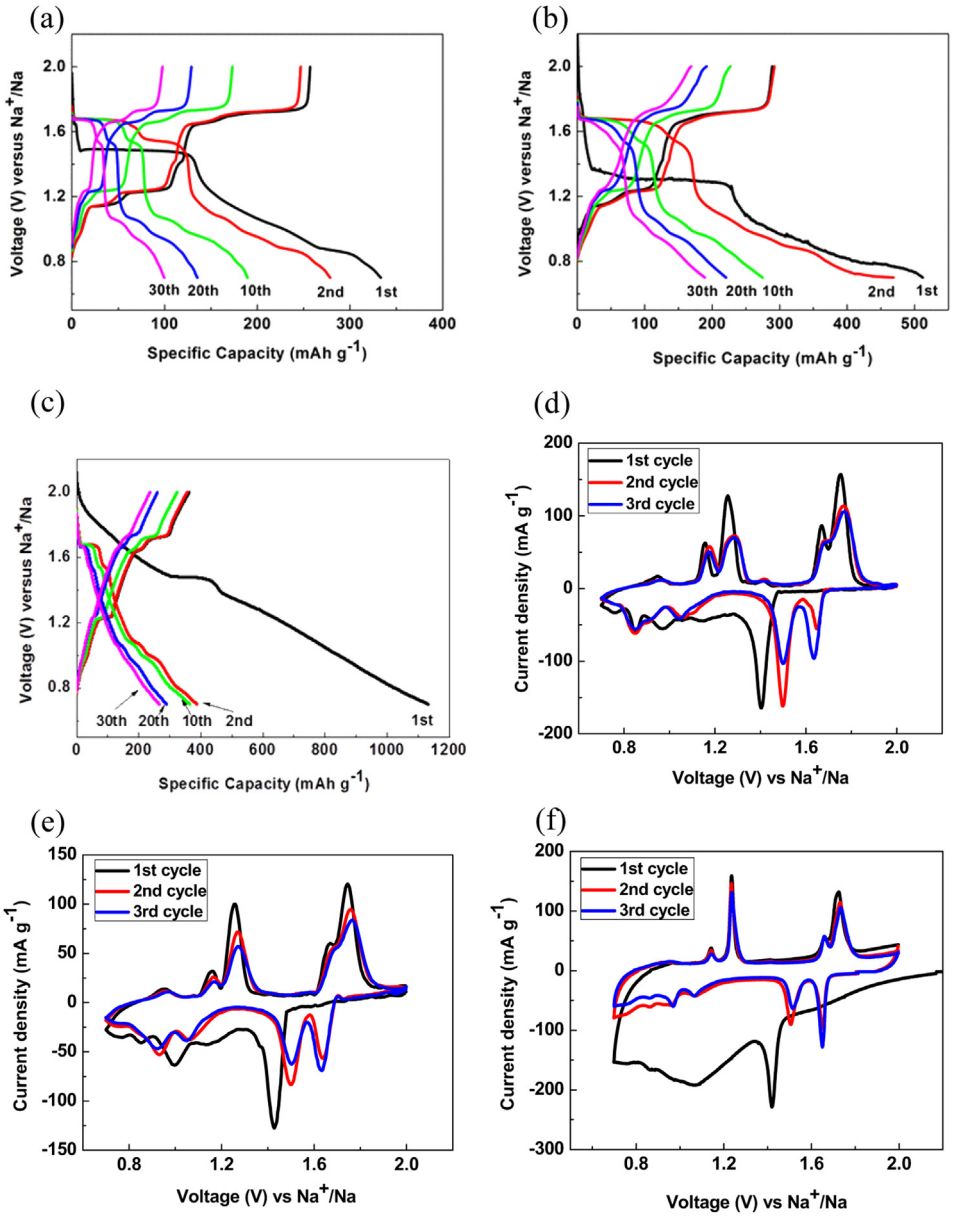

Fig. 4. Electrochemical performances of materials. The galvanostatic charge–discharge curves of pristine CADS (a), sCADS (b) and GO-CADS (c) between 0.7 V and 2.0 V versus Na/Na^+ at room temperature. Cyclic voltammograms of pristine CADS (d), sCADS (e) and GO-CADS (f) at 0.1 mV s^{-1} in the potential window from 0.7 V to 2.0 V versus Na/Na^+.

sodium ions enables CADS to be an electrode material for Na ion batteries.

Three CADS samples, micro-sized pristine CADS, submicrometer-size CADS (sCADS), and graphene oxide wrapped CADS (GO-CADS), were used to investigate the capacity decline mechanism. The sCADS particles were synthesized by dissolving pristine CADS into water, and then rapidly evaporating the CADS solution using the ultrasonic spray pyrolysis. The GO-CADSs were synthesized by rapidly drying the graphene oxide and CADS aqueous solution at 200 °C using the ultrasonic spray pyrolysis. The morphology of three CADS samples was characterized by scanning electron microscopy (SEM) as shown in Fig. 2. The pristine CADS consist of long bars and some irregular-structured particles which tend to aggregate to form micro-size particles (Fig. 2a). As shown in Fig. 2b, the sCADS particles have spherical morphology with the particle size of 0.5–1.0 μm, which is about ten times smaller than that of pristine CADS. Fig. 2c shows the SEM images of GO-CADS, in which all the CADS particles are encapsulated by the folded and wrinkled graphene oxide. The morphology of the GO-CADS composite is very uniform with particle size typically less than 1 μm, which is similar to sCADS. This is attributed to the unique ultrasonic spray pyrolysis. As water evaporates, the amphiphilic GO sheets would migrate to the surface of the droplets to form a shell. Since the diameter of the precipitated CADS particles was much smaller than that of the aerosol droplets, further water evaporation could collapse the GO shell, resulting in a crumpled morphology that encapsulates the CADS particles [17]. The transmission electron microscopy (TEM) images of GO-CADS in Fig. 3 also confirm that all the CADS particles are encapsulated by the folded and wrinkled graphene oxide. The energy-dispersive X-ray spectroscopy (EDS) elemental mapping images (Fig. 3c–e) reveal that CADS is uniformly distributed in the GO shell since sodium mapping image overlaps with carbon and oxygen mapping images. The content of CADS in GO-CADS is 37 wt% as determined by thermogravimetric

analysis (TGA) results for GO, CADS and GO-CADS as shown in Fig. S1 (Supporting information). The GO is treated by ultrasonic spray pyrolysis under the same condition as GO-CADS. For GO-CADS, the Na ion can penetrate through the defects and open-end of GO to react with the inner CADS [13].

The structures of three CADS samples are identified by the XRD. The XRD patterns of sCADS and GO-CADS are the same as the pristine CADS as shown in Fig. S2 (Supporting information), indicating that the sCADS, GO-CADS and pristine CADS have the same crystal structure. However, the XRD peak of pristine CADS is slightly sharper than that of sCADS and GO-CADS, demonstrating the crystalline structures of CADS were not well-developed due to rapid precipitation (1.0 s of residential time) in ultrasonic spray pyrolysis process.

3.1.1. Sodiation/desodiation behaviors

The charge/discharge behaviors of pristine CADS, sCADS and GO-CADS in different cycles at a current density of 20 mA g^{-1} are shown in Fig. 4. The voltage profiles of all three CADS samples show serials voltage plateaus and the potentials of first sodiation plateaus are lower than that in the subsequent sodiation process, demonstrating that all three CADS samples experience successive and reversible phase transformations during sodiation/desodiation and the stress/strain due to large volume expansion in the first sodiation induces a large strain overpotential. The large strain overpotential is significantly reduced in the subsequent cycles due to the introduction of defects in the first sodiation, shifting the potential back to a higher value after the first sodiation. The reason why sCADS has larger strain overpotential than pristine CADS in the first sodiation is because more Na ion (250 mAh g^{-1}) is inserted into sCADS in the first plateau than that (150 mAh g^{-1}) in pristine CADS. After the first charge/discharge cycle, minimization of the CADS particle size from 5–10 μm to 0.5–1.0 μm does not change the voltage plateaus (Fig. 4a and b), but the capacity (287.8 mAh g^{-1}) of sCADS is larger than that (246.7 mAh g^{-1}) of pristine CADS due to the reduced particle size and consequently improved kinetics of the former. The capacity of sCADS is very close to the theoretical capacity (288 mAh g^{-1}) of CADS, which is calculated based on one CADS molecule can react with two sodium ions. Since GO can reversibly react with Na^+, and deliver a reversible capacity of 39 mAh g^{-1} (Supporting information, Fig. S3), the initial capacity of CADS in GO-CADS after subtracting the capacity of GO is about 293 mAh g^{-1}, which is higher than theoretical capacity, probably due to the fact that carbon black additive is also active for Na ion storage. The high capacity of CADS in GO-CADS demonstrates that GO shell can effectively enhance the utilization of inside CADS due to the core shell structure and the higher conductivity of GO than CADS. The slight change in the voltage profile of GO-CADS compared with that of CADS is attributed to the sloping voltage curves of GO capsular [14]. The voltage plateaus and reaction reversibility of CADS, sCADS, GO-CADS can be more clearly observed in cyclic voltammogram profiles (Fig. 4d–f). In the first sodiation/desodiation cycle of CADS, there are three clear cathodic peaks at 1.42 V, 1.0 V, 0.85 V and a shoulder at 1.15 V, and four anodic peaks at 1.15 V, 1.25 V, 1.7 V and 1.8 V are also observed. However, the shoulder at 1.15 V disappears after the first cycle, and the cathodic peak at 1.42 V in the first cycle shifts to high voltage to split into two new peaks at 1.5 V and 1.65 V in the following cycles. This result suggests that the CADS experiences an activation process during the first sodiation, which has been observed in many high capacity electrodes with large volume changes such as Sn and Sb [15]. The activation process characterized by the high stain overpotential in the first sodiation process is induced by the high stress/strain raised by the first sodiation. The high stress/strain in the first sodiation generates a large amount of defects (cracks, dislocations, plastic deformations, etc) in host to release the strain/stress. Therefore, the relaxation of the strain/stress in the first sodiation decreases the overpotential, and the sodiation potential shifts back to more positive values in the following sodiation process. After the first cycle, there are four peaks in the desodiation scans, which are corresponding to the four peaks in the sodiation scans, demonstrating the high reversibility of sodiation and desodiation of CADS. The cyclic voltammograms of sCADS and GO-CADS are similar with pristine CADS. There is a broad shoulder at 1.1 V in the first sodiation process of GO-CADS owing to the irreversible reaction on the surface of GO. After the first sodiation, GO-CADS displays similar anodic and cathodic peaks as pristine CADS and sCADS. The highly reversible peaks in the cyclic voltammetry curves and the highly reversible plateaus in the galvanostatic charge–discharge curves suggest that CADS experiences highly reversible phase transformation during sodiation/desodiation.

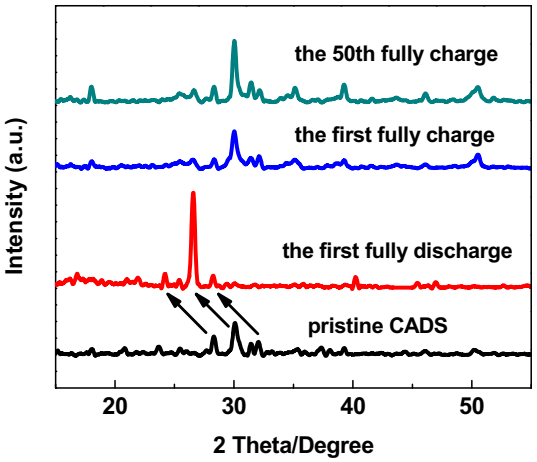

Fig. 5. The XRD patterns of pristine CADS (black line), the first fully discharged CADS (red line), the first fully charged CADS (blue line) and the 50th fully charged CADs (green line). (For interpretation of the references to color in this figure legend, the reader is referred to the web version of this article.)

The reversible phase change during sodiation/desodiation is also confirmed by XRD (Fig. 5). In the full sodiation state, the original peaks of pristine CADS at 28° and 30° shift to 24° and 26°. Moreover, the two peaks at ~32° of pristine CADS salt merge together to form a new peak at ~28° after full sodiation. Therefore, XRD data confirm the phase change of CADS during sodiation. After the desodiation, the XRD peaks of CADS shift back to their original positions, and maintain the positions after 50th full desodiations, illustrating that the phase transformation is highly reversible.

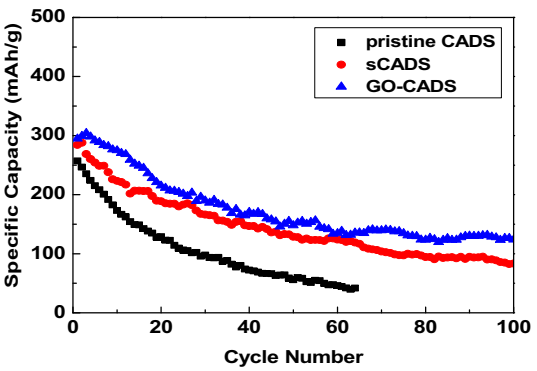

Fig. 6. Desodiation capacity versus cycle number (current density: 20 mA g^{-1}) for pristine CADS, sCADS and GO-CADS, respectively.

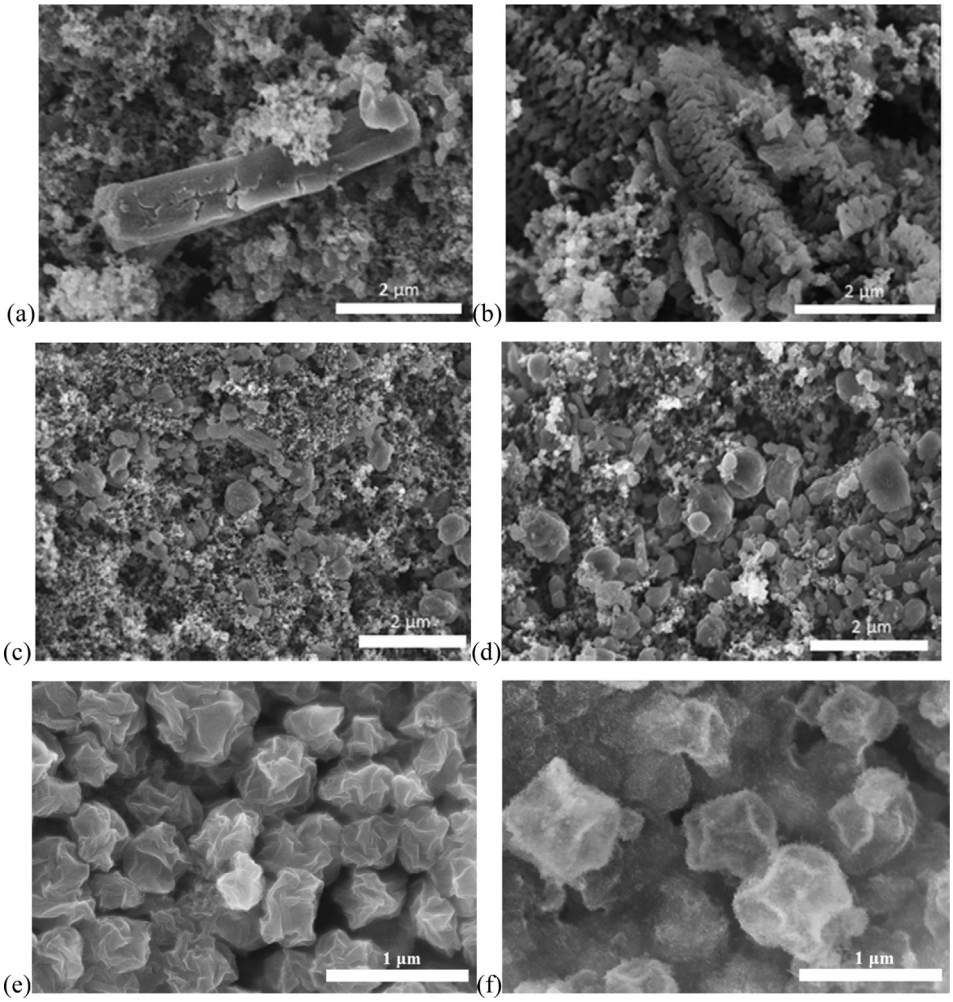

Fig. 7. SEM images of the pristine CADS electrode materials before test (a) and after 50 cycles (b); SEM images of the sCADS electrode materials before test (c) and after 50 cycles (d); SEM images of GO-CADS electrode materials before test (e) and after 50 cycles (f).

Comparing to pristine CADS, a few extra XRD peaks in desodiated CADS might imply the uncompleted phase transformation in the active material after it is charged to 2.0 V.

3.1.2. Cycling stability and mechanism for capacity decay

The cycling stability of three CADS samples was tested at a current density of 20 mA g^{-1} (Fig. 6). The capacity of pristine CADS quickly decreases from 250 mAh g^{-1} to 50 mAh g^{-1} after 60 cycles. If the dissolution of organic salts into organic electrolyte is responsible for the fast capacity decay, the capacity decline of sCADS should be much faster than pristine CADS due to the reduced particle size and thus enhanced contact surface between sCADS and electrolyte. However, the sCADS has much better cycling stability, demonstrating that the dissolution of CADS is not the major reason for the capacity decay. The insolubility of CADS in electrolyte is directly tested by comparing the Fourier transform infrared spectroscopy (FTIR) spectra of fresh electrolyte and the electrolyte after 50 sodiation/desodiation cycles. Fig. S4a shows the FTIR spectrum of CADS. There is a very sharp peak at 1500 cm^{-1} which represents the stretching vibration of the carbonyl groups and carbon–carbon double bond in CADS. If CADS dissolves in the electrolyte, there should be a peak at 1500 cm^{-1} in the FTIR spectrum of the electrolyte after 50 cycles, whereas the spectra of the electrolyte before test and after 50 cycles are nearly the same in the range from 800 to 2000 cm^{-1} in Fig. S4b. UV–vis spectroscopy is also employed to measure the active material in the electrolyte. As shown in Fig. S5, the UV–vis spectra of cycled electrolyte (50 cycles) are almost the same to that of the fresh electrolyte, indicating no active material is dissolved in the electrolyte during cycles. Thus, these evidences confirm that CADS is not dissolved in the electrolyte during the charge and discharge.

Another possibility for capacity decline is the pulverization of CADS particles due to the volume change induced by repeating phase transformation during sodiation/desodiation process. Pulverization-induced capacity decay has been observed in high capacity anodes such as Sn in Na-ion battery [16]. The pulverization of CADS particles will demolish the integrity of electrode structure, resulting in poor cycling stability. The morphology change of CADS before and after 50 sodiation/desodiation cycles is observed by SEM. As shown by SEM images in Fig. 7a and b, the pristine CADS in the electrode has the long bar-like shape, but after 50 cycles the long bar is severely cracked. The long bar is broken into numerous small fragmentations, most of which do not connect with conductive carbon. The most effective method to reduce the particle pulverization is to minimize the particle sizes [10]. Fig. 7c and d shows the SEM images of the fresh sCADS material and cycled sCADS. sCADS particles maintain the similar particle morphology after 50 cycles and no cracks are observed, thus the sCADS has much better cycling stability than CADS as demonstrated in Fig. 6. The GO encapsulation of sCADS can further enhance morphology

stability of sCADS as demonstrated in Fig. 7e and f. After 50 charge/discharge cycles, no obvious morphology change can be observed. The good morphology stability of GO-CADS is consistent with the best cycle life of GO-CADS electrode as shown in Fig. 6. The FTIR, UV–vis and SEM images in Figs. S4, S5 and Fig. 7 demonstrate that the capacity fading is not due to the dissolution of sCADS and GO-CADS in the electrolyte, but the large stress/strain of CADS during repeating phase changes.

Since the particle pulverization will isolate the small pulverized CADS particles from carbon additive and current collector during sodiation/desodiation process, the isolated CADS particles are not able to electrochemically react with Na^+ in the following cycles, thus dramatically decreasing the battery performance. However, if CADS particles are encapsulated by a conductive graphene oxides, the void in the crumpled graphene oxide coating can accommodate the volume expansion of CADS upon sodiation and maintain the connection between inner CADS particles and outer graphene oxide cover (even they are pulverized), thus improving cycling stability. As demonstrated in Fig. 6, the graphene oxide encapsulated CADS shows the best cycling stability. Further improvement for cycling stability is under investigation by optimizing the ratio of graphene oxide and CADS, increasing the aerosol spray temperature, and adjusting the residential time.

4. Conclusions

Croconic acid disodium salt, a carbonyl group based organic compound, was used as an anode material for the first time. It is shown that the rapid capacity fading of pristine CADS in sodium ion batteries is due to the particle pulverization rather than the dissolution in organic electrolyte. The CADS experiences a serial phase transformations during sodiation/desodiation process. The volume change during phase transformations triggers the particle pulverization, which is confirmed by SEM results. The sCADS and GO-CADS fabricated by ultrasonic spray pyrolysis have much smaller particle size than pristine CADS, and provide much better cycling stability due to the suppression of pulverization and improvement of electronic conductivity. Hence, minimizing the CADS particle size and encapsulating CADS particles by graphene oxide are two effective methods to enhance the electrochemical performance of CADS.

Acknowledgments

This work was supported by the Army Research Office under Contract No.: W911NF1110231. We acknowledge the support of the Maryland NanoCenter and its NispLab. The NispLab is supported in part by the NSF as a MRSEC Shared Experimental Facility. We acknowledge Dr. Kai Zhong, Guoqiang Jian, Kaitlyn Crawford and Prof. Lawrence R. Sita for their technique support.

Appendix A. Supplementary data

Supplementary data related to this article can be found at http://dx.doi.org/10.1016/j.jpowsour.2013.10.131.

References

[1] (a) V. Palomares, P. Serras, I. Villaluenga, K.B. Hueso, J. Carretero-González, T. Rojo, Energy Environ. Sci. 5 (2012) 5884–5901;
(b) M.D. Slater, D. Kim, E. Lee, C.S. Johnson, Adv. Funct. Mater. 23 (2013) 947–958.
[2] (a) Y. Zhu, Y. Xu, Y. Liu, C. Luo, C. Wang, Nanoscale 5 (2013) 780–787;
(b) Y. Xu, Q. Liu, Y. Zhu, Y. Liu, A. Langrock, M.R. Zachariah, C. Wang, Nano Lett. 13 (2013) 470–474;
(c) A. Abouimrane, D. Dambournet, K.W. Chapman, P.J. Chupas, W. Weng, K. Amine, J. Am. Chem. Soc. 134 (2012) 4505–4508.
[3] Y. Liang, Z. Tao, J. Chen, Adv. Energy Mater. 2 (2012) 742–769.
[4] H. Chen, M. Armand, G. Demailly, F. Dolhem, P. Poizot, J. Tarascon, ChemSusChem 1 (2008) 348–355.
[5] (a) B. Genorio, K. Pirnat, R. Cerc-Korosec, R. Dominko, M. Gaberscek, Angew. Chem. Int. Ed. 49 (2010) 7222–7224;
(b) Z. Song, H. Zhan, Y. Zhou, Angew. Chem. Int. Ed. 49 (2010) 8444–8448;
(c) Z. Song, T. Xu, M.L. Gordin, Y. Jiang, I. Bae, Q. Xiao, H. Zhan, J. Liu, D. Wang, Nano Lett. 12 (2012) 2205–2211;
(d) Y. Morita, S. Nishida, T. Murata, M. Moriguchi, A. Ueda, M. Satoh, K. Arifuku, K. Sato, T. Takui, Nat. Mater. 10 (2011) 947–951;
(e) J. Geng, J. Bonnet, S. Renault, F. Dolhem, P. Poizot, Energy Environ. Sci. 3 (2010) 1929–1933.
[6] H. Chen, M. Armand, M. Courty, M. Jiang, C.P. Grey, F. Dolhem, J. Tarascon, P. Poizot, J. Am. Chem. Soc. 131 (2009) 8984–8988.
[7] W. Walker, S. Grugeon, O. Mentre, S. Laruelle, J. Tarascon, F. Wudl, J. Am. Chem. Soc. 132 (2010) 6517–6523.
[8] M. Armand, S. Grugeon, H. Vezin, S. Laruelle, P. Ribière, P. Poizot, J. Tarascon, Nat. Mater. 8 (2009) 120–125.
[9] X. Chen, K. Gerasopoulos, J. Guo, A. Brown, C. Wang, R. Ghodssi, J.N. Culver, Adv. Funct. Mater. 21 (2011) 380–387.
[10] U. Kasavajjula, C. Wang, A.J. Appleby, J. Power Sources 163 (2007) 1003–1039.
[11] (a) Y. Park, D. Shin, S.H. Woo, N.S. Choi, K.H. Shin, S.M. Oh, K.T. Lee, S.Y. Hong, Adv. Mater. 24 (2012) 3562–3567;
(b) L. Zhao, J. Zhao, Y. Hu, H. Li, Z. Zhou, M. Armand, L. Chen, Adv. Energy Mater. 2 (2012) 962–965;
(c) A. Abouimrane, W. Weng, H. Eltayeb, Y. Cui, J. Niklas, O. Poluektov, K. Amine, Energy Environ. Sci. 5 (2012) 9632–9638.
[12] K. Okuyama, I.W. Lenggoro, Chem. Eng. Sci. 58 (2003) 537–547.
[13] B. Xu, S. Yue, Z. Sui, X. Zhang, S. Hou, G. Cao, Y. Yang, Energy Environ. Sci. 4 (2011) 2826–2830.
[14] J. Luo, X. Zhao, J. Wu, H.D. Jang, H.H. Kung, J. Huang, J. Phys. Chem. Lett. 3 (2012) 1824–1829.
[15] Y. Wen, Y. Zhu, A. Langrock, A. Manivannan, S.H. Ehrman, C. Wang, Small (2013), http://dx.doi.org/10.1002/smll.201202512.
[16] Y. Wang, S. Chou, H. Liu, S. Dou, Carbon 57 (2013) 202–208.
[17] (a) Y. Xu, Y. Zhu, Y. Liu, C. Wang, Adv. Energy Mater. 3 (2013) 128–133;
(b) Y. Zhu, X. Han, Y. Xu, Y. Liu, S. Zheng, K. Xu, L. Hu, C. Wang, ACS Nano (2013), http://dx.doi.org/10.1021/nn4025674.